Recent Advances in Thermal Mechanically Coupled Analysis using MSC

Ted B. Wertheimer, PhD; MSC.Software ted.wertheimer@mscsoftware.com
Sean Harvey; MSC.Software sean.harvey@mscsoftware.com
Robert Minaie, PhD; Wichita State University bob.minaie@witchita.edu

ABSTRACT
The MSC family of products including MD Nastran, Marc and Sinda provide advanced capabilities for the solution of complex heat transfer and thermal stress analysis is a multi-disciplinary environment. This permits the simulation of thermal problems, including manufacturing environment, conventional use and treatment of thermal protection systems. This paper will discuss the application of these products in a variety of novel aerospace applications including curing simulation, welding, shape memory actuators, and thermal contact. In the first three applications the material undergoes a phase change during the coupled simulation which has a significant influence on the thermal and structural behavior.

Curing Simulation

Composite materials are becoming prevalent in airplanes from large commercial vehicles such as the Airbus 350 and the Boeing 787 to smaller jets from Bombardier, Embraer and Hawker Beechcraft. To achieve the high level of quality in the manufacturing of these composite structures curing simulation is performed to predict the amount of shrinkage that will occur, the amount of residual stresses and potential spring back of the part using the Marc program. A coupled thermal-mechanical analysis is performed to incorporate the effects of the cure kinematics on the thermal and structural behavior. To perform such an analysis one is required to have a good knowledge of the temperature dependent thermal and structural properties. Furthermore the thermal and mechanical properties may be a function of the degree of cure as well. The degree of cure is based upon one of the well known cure kinematics equations shown in Table 1 [1].

The heat flux is obtained from

$$\dot{Q}=\frac{d\alpha}{dt}(1-V_f)\rho_r H_r$$

Where H_r is the resin degree of cure and V_f is the fiber volume fraction.

The thermal-mechanically coupled procedure can be characterized as shown in Figure 1.

It must be recognized that in the mechanical simulation four phenomena occur that influence the results

1. Thermal strains in the material
2. Material shrinkage
3. Temperature dependent structural properties
4. Viscoelastic behavior of the material.

Table 1. – Cure kinematic models.

Model	Equations	Parameters
Model 1 Lee, Loos and Springer (1982)	$\frac{d\alpha}{dt} = (K_1 + K_2\alpha)(1-\alpha)(B-\alpha)$ $\alpha \le \alpha_c$ $\frac{d\alpha}{dt} = K_3(1-\alpha)\ \alpha > \alpha_c$ $K_i = A_i e^{-\Delta E_i/(RT)}$	A_1, A_2, A_3, ΔE_1, ΔE_2, ΔE_3, B, α_C, H_R
(Included in Model 2) Lee, Chiu, and Lin (1992); White and Hahn (1992)	$\frac{d\alpha}{dt} = K\alpha^m(1-\alpha)^n$ $K = Ae^{-\Delta E/(RT)}$	A, ΔE, m, n, H_R
(Included in Model 2) Kenny (1992) Scott (1991)	$\frac{d\alpha}{dt} = K(1-\alpha)^n$ $K = Ae^{-\Delta E/(RT)}$	A, ΔE, n, H_R
Model 2 (combined Model) Scott (1991)	$\frac{d\alpha}{dt} = (K_1 + K_2\alpha^m)(1-\alpha)^n$ $K_i = A_i e^{-\Delta E_i/(RT)}$	A_1, A_2, ΔE_1, ΔE_2, m, n, H_R
Model 3 Lee, Chiu, and Lin (1992)	$\frac{d\alpha}{dt} = K_1(1-\alpha)^l + K_2\alpha^m(1-\alpha)^n$ $K_i = A_i e^{-\Delta E_i/(RT)}$	A_1, A_2, ΔE_1, ΔE_2, l, m, n, H_R
Model 4 Johnston and Hubert (1995)	$\frac{d\alpha}{dt} = \frac{K\alpha^m(1-\alpha)^n}{1 + e^{C\{\alpha-(\alpha_{C0}+\alpha_{CT}T)\}}}$ $K_i = A_i e^{-\Delta E_i/(RT)}$	A, ΔE, m, n, C, α_{C0}, α_{CT}, H_R

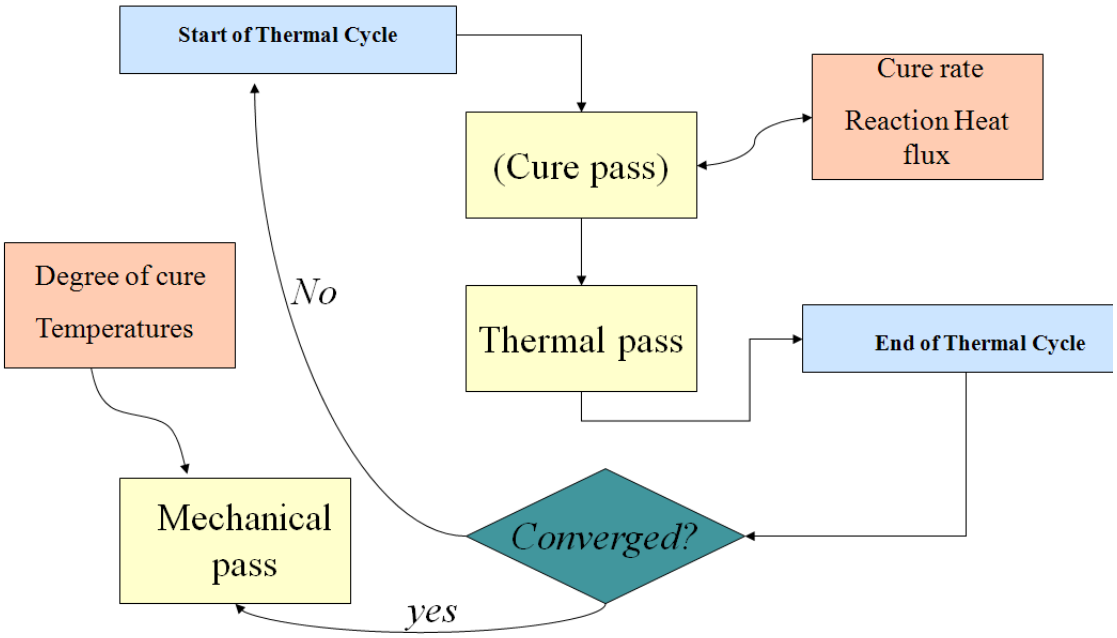

Figure 1: Coupled Curing Analysis Flow Path

This is complicated because the composite material is anisotropic. The material data may be entered either using tables (with multiple independent variables) or through user subroutines. In previous simulations some of these effects were neglected. Cure shrinkage is governed by one of two empirical models given in Table 2.

Table 2. Cure Shrinkage models

Model	Equations	Parameters
Model 1 Bogetti and Gillespie (1992) [Ref. 42]	$V_r^S = 0.0$ $\quad \alpha < \alpha_{C1}$ $V_r^S = A*\alpha_S + (V_r^{S\infty} - A)*\alpha_S^2$ $\quad \alpha_{C1} \le \alpha < \alpha_{C2}$ $V_r^S = V_r^{S\infty}$ $\quad \alpha \ge \alpha_{C2}$ $\alpha_S - \frac{\alpha - \alpha_{C1}}{\alpha_{C2} - \alpha_{C1}}$	V_r^S, α_{C1}, α_{C2}, A
Model 2 White and Hahn 1992 [Ref. 48]	$V_r^S = V_r^{S\infty} * 10^{B(\alpha - \alpha_c)}$ $\quad \alpha \le \alpha_C$ $V_r^S = V_r^{S\infty}$ $\quad \alpha > \alpha_C$	$V_r^{S\infty}$, α_C, B

In these simulations an 8-node composite continuum element is used. Using the Springer-Loos model excellent correlation is obtained as shown in Figure 2 [2]. In a similar manner the Bogetti model gave very good correlation with experiment as shown in Figure 3.

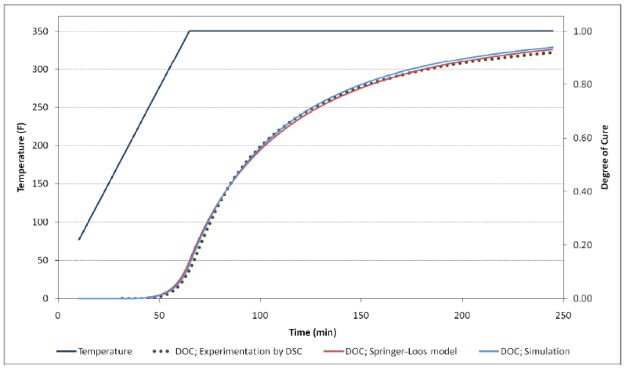

Figure 2: Experimental and numerical Simulation of degree of cure.

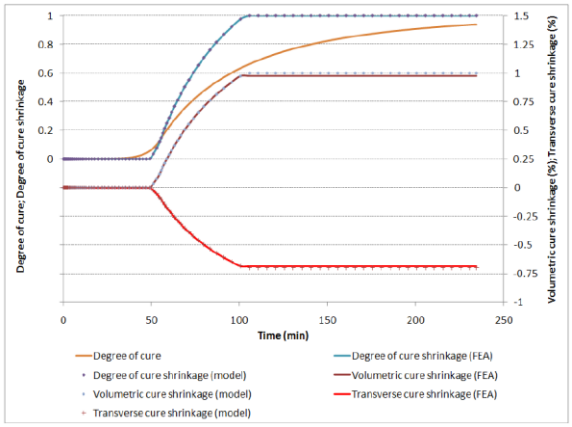

Figure 3: Experimental and numerical simulation of cure shrinkage.

Four panels were cured using the manufacturer's recommended curing cycle (MRCC) with a stacking sequence shown in table 3 and the distortion was measured using a laser scanning technique at the National Institute for Aviation Research (NIAR). The panels are formed on a flat aluminum tool.

Table 3 – Stacking sequence of four panels

Panel No.	Panel Type	Stacking sequence	Size (in x in)
1	Asymmetric, balanced	$[0/45/90/-45]_4$	17x17
2	Symmetric, balanced	$[0/45/90/-45]_{2S}$	17x17
3	Symmetric, unbalanced	$[0/45/90/45]_{2S}$	17x17
4	Asymmetric, unbalanced	$[0/45/90/45]_4$	17x17

Comparison of the distortion between the simulation and experiment are shown in Figure. 4. A good agreement was observed between the numerical simulation and experiment both in terms of maximum distortion and the pattern of the 3-d distortion. An advantage of the numerical procedure is that parametric studies may be done quickly to determine the effect of the process variables such as the curing temperature and pressure cycle. Furthermore the tooling may be designed to compensate for the curing distortion such that the finished product satisfies the design requirements.

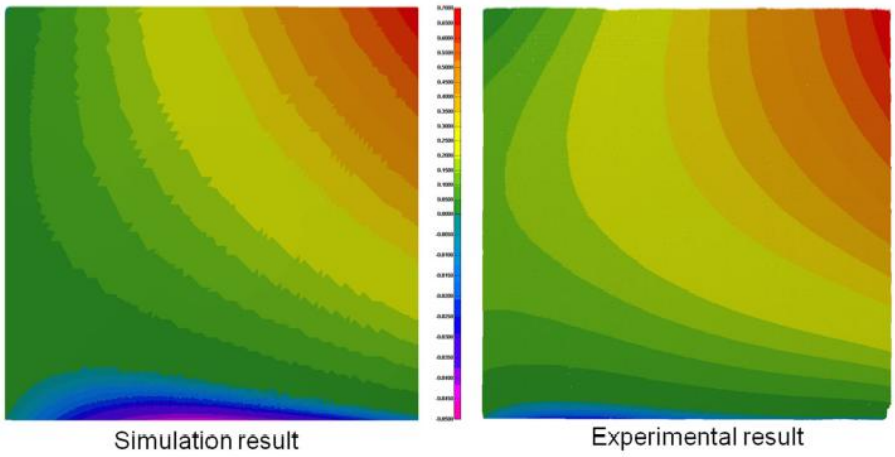

Comparison of distortion between simulation result and experimentation for Panel 1

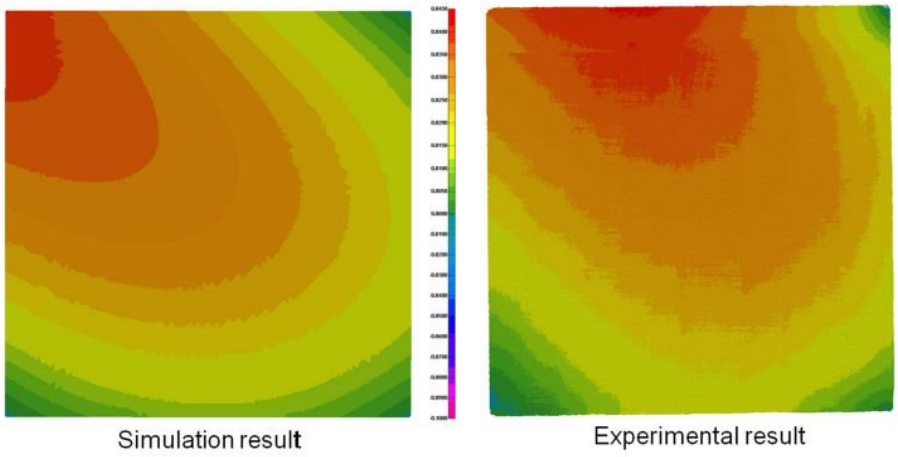

Comparison of distortion between simulation result and experimentation for Panel 2

Figure 4: Distortion Correlation between Simulation and Experiment

Shape Memory Actuator

Micro actuators are often used in control systems; this section illustrates the coupled transient solution of the electrical, thermal, and mechanical behavior of a shape memory alloy (SMA) actuator. Specifically, a voltage potential is applied over the finite element mesh of the device, and current flows through the actuator wires and sliders in series. Due to the resistivity of the SMA, the material heats and causes the SMA actuator wires to undergo the well known shape recovery as the material phase transforms to austenite. This strain causes mechanical motion of the SMA, and resulting motion of the attached actuator sliders occurs. Cooling of the device due to thermal conduction and convection, along with a return spring, bring the actuator sliders back to their starting positions, as the material phase transforms back to martensite. The finite element analysis solver is able to calculate relevant quantities, including, but not limited to voltage, current, temperature, strains, stresses, resulting motions and forces of the actuator.

Material nonlinearities, geometric nonlinearities, and contact nonlinearities between mating components are all included in the solution. The resulting actuator's stroke, actuation times, cool/return time, and output force capability are compared to physically measured data from a commercially available small scale SMA actuator for validation. The actuator investigated is shown in Figure 5.

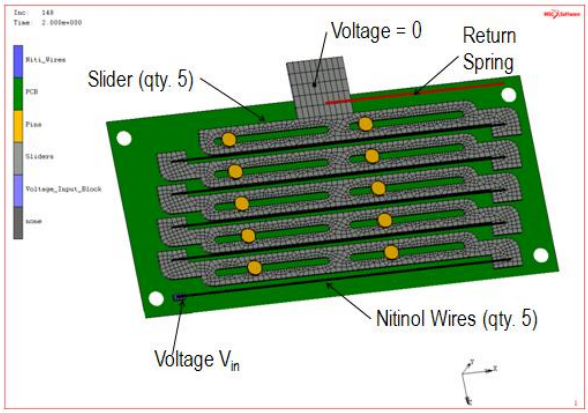

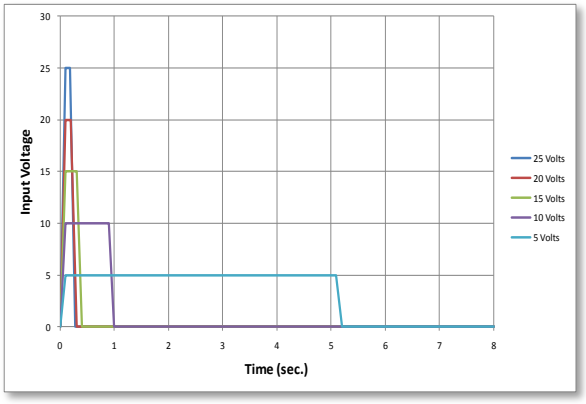

Figure 5: Actuator Geometry

Figure 6: Applied Voltage

The actuator is made of Nitinol which exhibits a reversible, thermoelastic transformation between a high-temperature, ordered cubic (B2) austenitic phase and a low-temperature, monoclinic (B19) martensitic phase. The Marc and Nastran programs incorporate a thermo-mechanical shape memory allow material model based upon the work of Saeedvafa and Asaro [3,4],The shape memory model requires additional material data as given in Table 4.

Table 4. Nitinol Material Data

Nitinol Thermo-Mechanical Constitutive Parameters			
Description	***Value***	***Description***	***Value***
Young's Modulus - Martensite	83,000 MPa	*Resistivity*	0.0008 Ohm mm
Young's Modulus - Austenite	41,000 MPa	*Deviatoric Transformation Strain*	0.085
Poisson's Ratio	0.33	*Volumetric Transformation Strain*	0.0
Density	6.45E-9 Mg/mm³	*Twinning Stress*	100 MPa
Martensite Start Temperature	36 °C	*g-A*	-4.0
Martensite Finish Temperature	24 °C	*g-B*	2.0
Austenite Start Temperature	54 °C	*g-C*	0.0
Austenite Finish Temperature	71 °C	*g-D*	2.8
Thermal Conductivity	0.0086 W/mm °C	*g-0*	300.0 MPa
Specific Heat	837,000 Joule/ Mg °C	*g-max*	1.0
Thermal Expansion Coefficient - Martensite	6.6E-6 mm/mm°C	*stress at g-max*	1.00E+20
Thermal Expansion Coefficient - Austenite	1.1E-5 mm/mm°C		

A commercially available shape memory actuator is simulated [5]. The initial voltage distribution and resultant temperature are shown below in Figure 7 and 8. The initial temperature is 20 C; hence the material is in a Martensite state. The temperature increases to 220C, where the material is completely in and Austenite state.

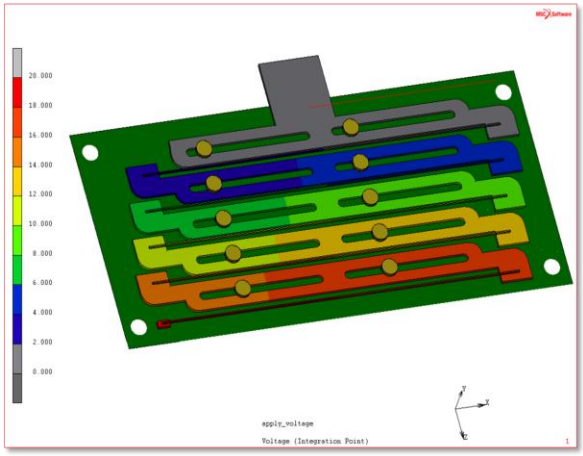

Figure 7: Voltage Distribution

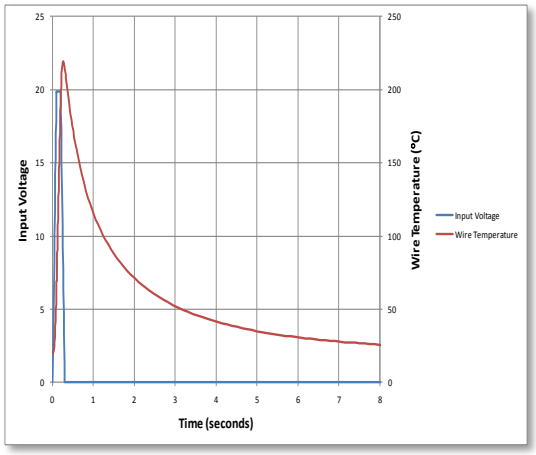

Figure 8: Temperature History

One can observe in Figure 9 that the actuator displacement is dependent upon the applied voltage. The stroke force is shown in Figure 10.

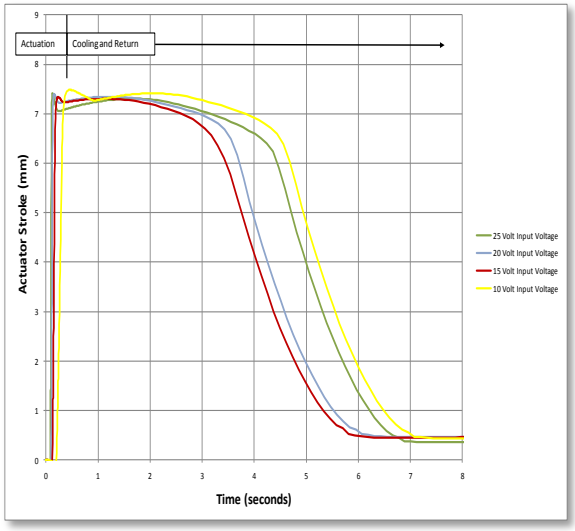

Figure 9: Stroke based upon applied voltage

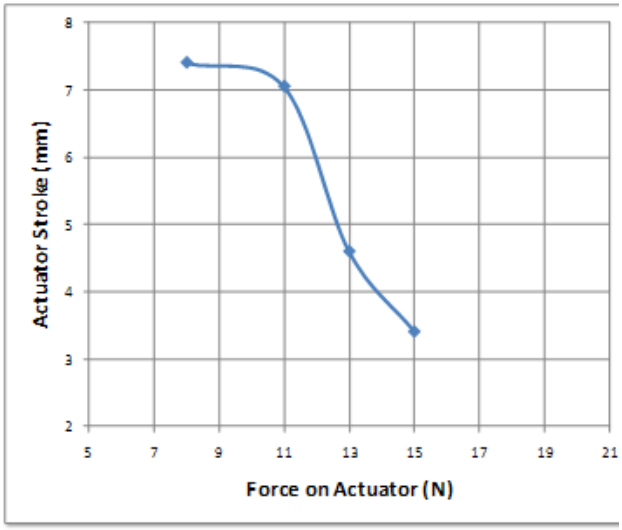

Figure 10: Force vs. Actuator

The correlation between the measured data and finite element calculation is shown in Figure 11. The results indicate that there is good correlation.

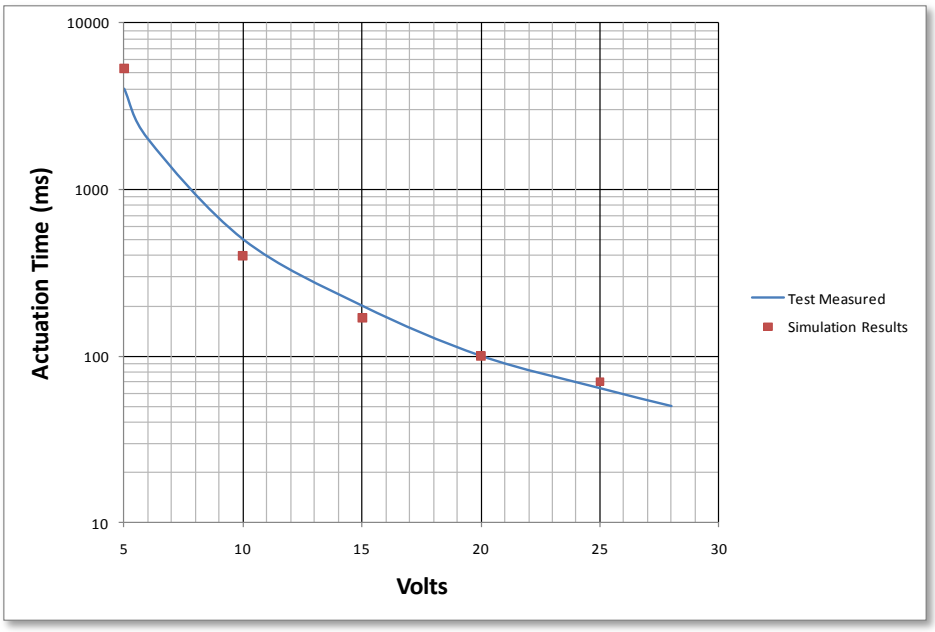

Figure 11: Numerical Correlation with Experiments.

Welding Simulation

Welding is an important connecting process in aerospace structures and has been the subject of many simulations. Welding techniques include spot, laser and friction stir welding, the later becoming more prevalent in aluminum aerospace structures. Welding simulation requires numerical procedures that are often not available in conventional simulations because of the following phenomena:

1. Metallurgical model to represent phase changes encountered
2. Moving boundary conditions associated with heat or mechanical source
3. Nonuniform thermal flux; requiring specific models or user subroutines.
4. High thermal gradients, requiring local adaptive meshing.
5. Weld bead ; requiring mesh activation
6. Residual stress calculations

Metallurgical models can be simplified based upon latent heat models, or user subroutines may be used to represent the phase change in the vicinity of the weld pool. The WELD PATH which can use used to define an arbitrary path as shown in Figure 12. The WELD FLUX option can be used to specify a thermal flux model based upon either the Pavelic disc or the Goldak's double ellipsoidal model shown in Figure 13. Finally the WELD FILER option may be used to control the addition of material for single or multi-pass weld path. Because of the high gradients a local adaptive meshing is used as shown in Figure 14. After the heat source leaves a region the element refinement is reversed. This is necessary for three dimensional analyses as otherwise the computational costs would be prohibitive. Because of the mesh adaptivity it is often expedient to

perform a thermal-mechanically coupled analysis as shown in Figure 15. Figure 16 shows the numerical and experimental correlation for the analysis of electron beam welding of Inconnel 718 [6].

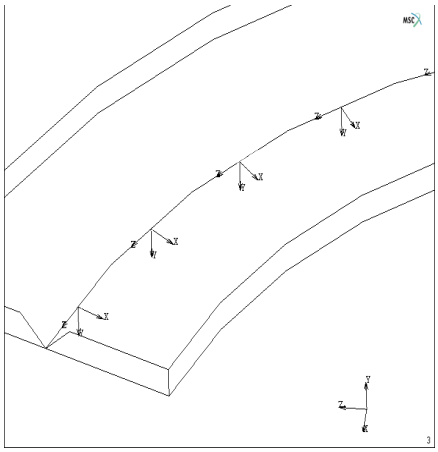

Figure 12: Weld Path definition

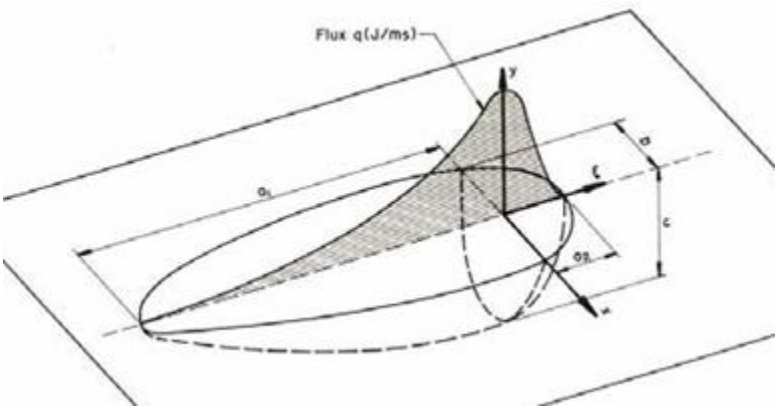

Figure 13: Double ellipsoid thermal

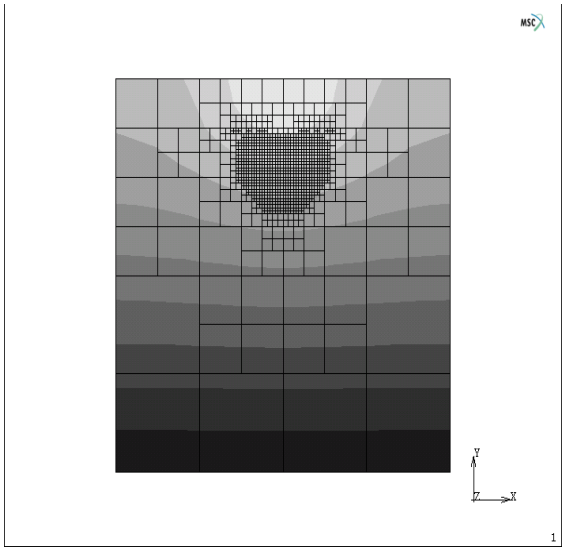

Figure 14: Mesh adaptivity due to gradients

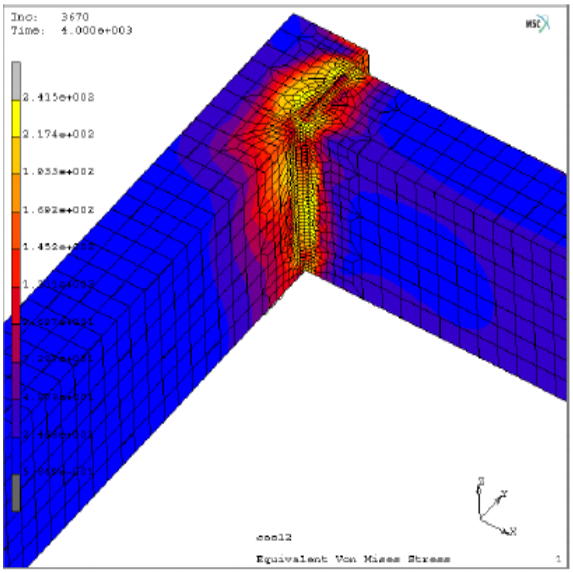

Figure 15: Residual stress calculations

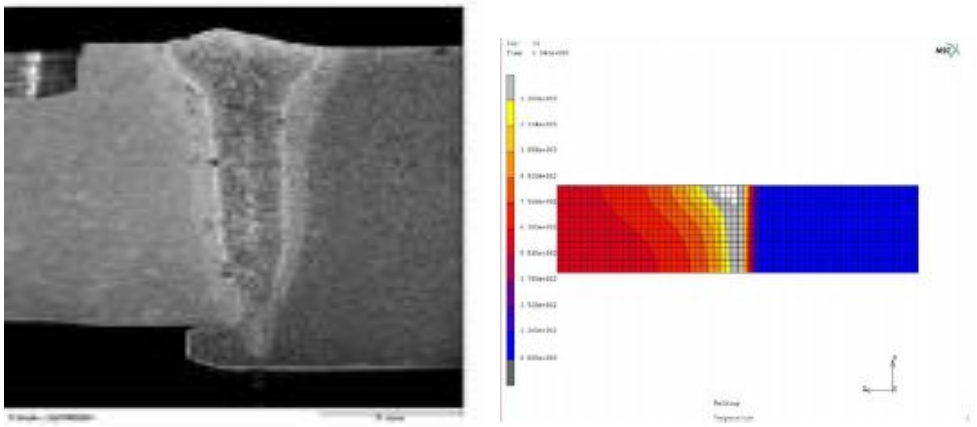

Figure 16: Experimental and numerical correlation

Nastran Coupled Simulation

The release of MD Nastran 2010 has introduced several new capabilities for the advanced thermal user including:

1. Heat transfer composite elements with multiple layers through the thickness. The temperature distribution may be either linear or quadratic through the thickness.
2. Easy-to-use thermal contact to allow assembly modeling without the requirement of congruent meshes
3. Uncoupled thermal stress analysis within the same job, by chaining a heat transfer analysis with a structural analysis.
4. Uncoupled thermal stress analysis where different meshes are used between the heat transfer simulation and the structural simulation and the results are spatially interpolated automatically. This capability includes transient simulation where the adaptive time stepping procedures do not need to align.
5. The Sinda product has been integrated with MD, so that a common user interface may be used for both the finite element formulation and the RC network procedure.
6. Coupled thermal – mechanical analysis is now available in MD Nastran.

As an example of temperature mapping in the Figure 17, where one can observe that at the trailing edge the mesh is different.

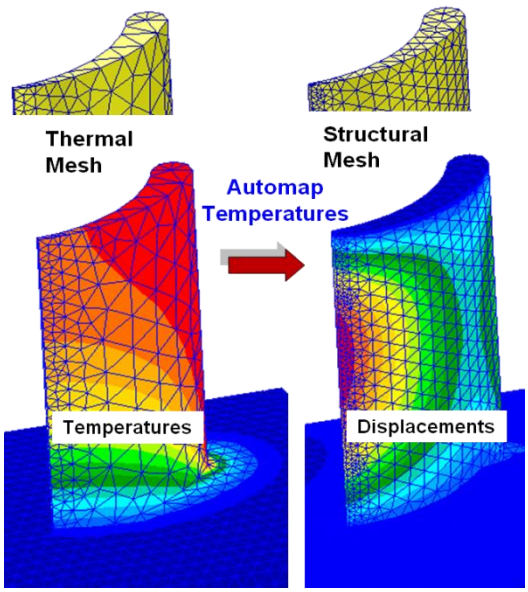

Figure 17: Mapping of temperatures when different meshes are used.

Thermal mechanical coupled analysis including contact has been well established for manufacturing simulations[7]. This capability has now been exposed in MD Nastran 2010 and is demonstrated for an axisymmetric billet compressed by two tools as shown in Figure 18. An axisymmetric model is used and due to symmetry only half is modeled. A modified triangular element is used which satisfies the nearly incompressible condition associated with plasticity. The material is elastic-plastic with temperature dependent properties. Heat is generated due to the plasticity and due to the friction between the two surfaces. 90% of the plastic work is converted to heat. The coefficient of friction is 0.65. There is a heat transfer coefficient between the billet and the environment and the billet and the tools. The billet is reduced in height from 30 mm to 20 mm. The temperatures are shown in Figure 19. The comparison of the temperature history with the reference solution is shown in Figure 21[8].

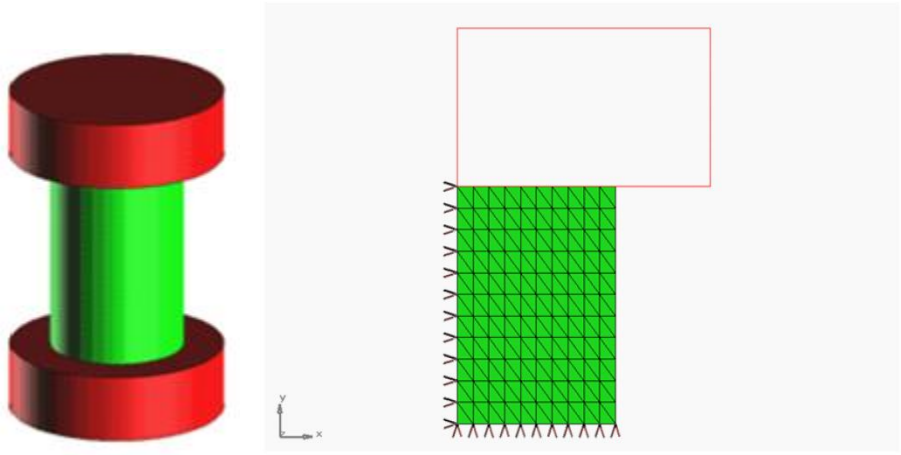

Figure 18: Model and finite element representation

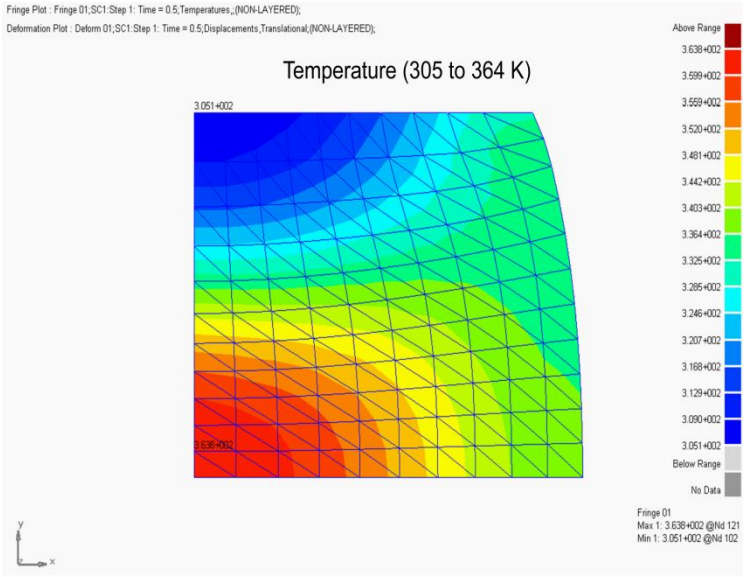

Figure 19 – Temperature distribution on deformed workpiece

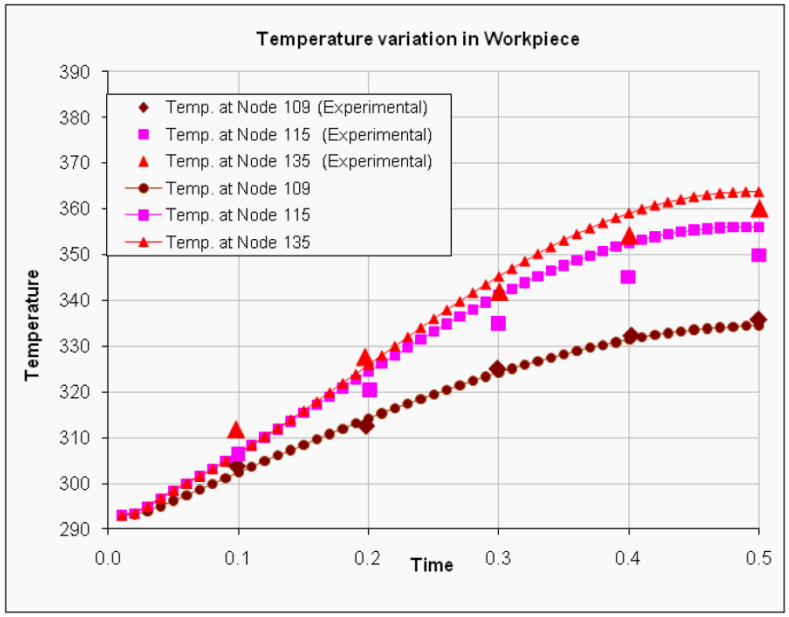

Figure 20– Temperature history – comparison with experiment

Conclusions

The finite element method can be successfully applied to a variety of thermally mechanically coupled aerospace problems. When used in conjunction with modern computing techniques this provides greater insight into the physical behavior and may be used to improve the design and safety of the system.

References

[1] Marc 2010 Volume A: Theory and User Information, MSC.Software Corporation, 2010, Santa Ana, CA.

[2] Minaie, Bob, Violette, Melanie, Large Scale Tooling Prediction for Composite Structures, Annual Report for FY 2010 for NIS Project 10-040, Whichita State University, 2010, Wichita, KS

[3]Saeedvafa, M, "A Constitutive Model for Shape Memory Alloys", Internal MSC Report, (January 2002).

[4] Saeedvafa M., and Asaro, R.J., LA-UR-95-482, Los Alamos Report, (1995).
Miyazaki, S., Otsuka, K., Suzuki, S. 1981. Transformation pseudoelasticity and deformation behavior in a Ti-50.6at%Ni alloy. *Scripta Metallurgica,* 15 (3); 287-292.

[5] Application Notes MigaOne TM On Board Actuators, June 2007, www.migamotors.com, accessed February 2010.

[6] Lundbäck, A.; Runnemalm, H., Validation of a Three-Dimensional Finite Element Model in Electron Beam Welding of Inconnel 718, Sience and Technology of Welding and Joining, Vol 10, no 6, 2005 pp 717-724

[7] Wertheimer,T. Thermal Mechanically Coupled Analysis in Metal Forming Procesesses. Numerical Methods in Industrial Forming Processes, Pinerigde Press, Swansea, U.K. 1982

[8] N.Rebelo and S.Kobayashi: "A Coupled Analysis of Viscoplastic Deformation and Heat Transfer – II", Int.J.Mech.,Sci. Vol.22, pp.707-718